Journal of Solid State Chemistry 183 (2010) 150–156

Contents lists available at ScienceDirect

Journal of Solid State Chemistry

journal homepage: www.elsevier.com/locate/jssc

Sandwich-type polyoxotungstate hybrids decorated by nickel-aromatic amine complexes

Peng-Tao Ma, Jun-Wei Zhao, Jing-Ping Wang **, Yue Shen, Jing-Yang Niu *

Institute of Molecular and Crystal Engineering, College of Chemistry and Chemical Engineering, Henan University, Kaifeng 475004, China

ARTICLE INFO

Article history:
Received 17 July 2009
Received in revised form
23 October 2009
Accepted 1 November 2009
Available online 10 November 2009

Keywords:
Polyoxometalate
Hydrothermal reaction
Nickel
Sandwich structure
Organoamine

ABSTRACT

Three new sandwich-type polyoxotungstates (POTs) decorated by nickel-2,2′-bpy complexes [{Ni(2,2′-bpy)$_2$(H$_2$O)}$_2${Ni(2,2′-bpy)}$_2$ {Ni$_4$(H$_2$O)$_2$(B-α-XW$_9$O$_{34}$)$_2$}]$^{n-}$ (X=P^V, n=4 for **1**; X=As^V, n=4 for **2**; X=Ge^{IV}, n=4 for **3**) (2,2′-bpy=2,2′-bipyridine) were successfully synthesized under hydrothermal conditions and structurally characterized by elemental analyses, IR spectroscopy, single-crystal X-ray diffraction, and magnetic properties. Single-crystal structural analyses indicate that **1** and **2** are isostructural and both crystallize in the monoclinic space group $C2/c$, whereas **3** belongs to the triclinic space group $P\bar{1}$. To our knowledge, **1**, **2** and **3** represent rare examples of the organic–inorganic hybrid sandwich-type polyoxometalates functionalized by multiple nickel-aromatic amine complexes. Magnetic measurements of **1** exhibit the presence of ferromagnetic interactions within the rhombic tetranuclear-Ni^{II} cluster.

1. Instruction

Currently, polyoxometalates (POMs) have been attracting considerable attention because of their exciting and unexpected structural variety combined with a multitude of potential applications in analytical science, materials science, catalysis, and medicine and in the emerging areas of bio- and nanotechnology [1–14]. In this field, an increasing research interest is to functionalize and decorate inorganic POMs by means of various organic ligands and/or transition-metal complexes (TMCs) to prepare inorganic–organic composite POM materials with unique structures and properties [15–20]. Thus, a large number of novel POM-based inorganic–organic composite functional compounds have been successfully obtained, which exhibit interesting electrochemical and magnetic properties [21,22].

Sandwich-type polyoxotungstates (POTs) represent a large subfamily of transition-metal substituted polyoxometalates (TMSPs), which are often easily synthesized by the self-assembly reaction of transition-metal (TM) ions with appropriate lacunary POT precursors (such as [XW$_9$O$_{34}$]$^{n-}$ or [X_2W$_{15}$O$_{56}$]$^{n-}$). To date, most of the obtained sandwich-type POTs are inorganic [23–32], however, sandwich-type species decorated by organic groups or TMCs are very rare [33–38]. Very recently, much more attention has been focused on the reactions of lacunary polyoxoanions with organic groups or TMCs, because this route can result in (1) novel sandwich-type POMs functionalized by organic substrates or TMCs; (2) high-nuclear TM cluster sandwiched POM aggregates; (3) multi-dimensional extended frameworks constructed from sandwich-type POM units and TMCs. In 2006, our group, for the first time, communicated a novel 1-D chain-like architecture built by Weakley sandwich-type germanotungstates and Cu^{II}-en cation bridges [33]. In 2007, Yang's group reported a series of two-dimensional frameworks constructed from tetra-TM sandwiched POTs with TM-organic cation bridges [34,35]. Very recently, Wang et al. addressed two extended structures consisting of sandwich-type POTs functionalized by aliphatic amines [36]. These reported sandwich-type POM-organic hybrids mostly were decorated by TM-aliphatic amine complexes. In these sandwich-type hybrids, TM-aliphatic amine complexes are incorporated in the sandwich belt, act as decorated cations coordinating to the surface oxygen atoms of POM matrixes, or function as bridges to construct multi-dimensional extended frameworks. However, the investigation on sandwich-type POTs decorated by TM-aromatic amine complexes is undeveloped. Recently, we began to explore this domain, as expected, four novel sandwich-type germanotungstates decorated by aromatic amines or TM-aromatic amine complexes {[Cu(2,2′-bpy)]$_2$[Cu(2,2′-bpy)$_2$]$_2$[Cu$_6$(2,2′-bpy)$_2$(B-α-GeW$_9$O$_{34}$)$_2$]}, {[Cu(phen)]$_2$[Cu(phen)$_2$]$_2$[Cu$_6$(phen)$_2$(B-α-GeW$_9$O$_{34}$)$_2$]}, [Co$_2$(2,2′-bpy)$_2$Co$_4$(H$_2$O)$_2$(B-α- GeW$_9$O$_{34}$)$_2$]$^{8-}$ and [{Mn(phen)}$_2$Mn$_4$(H$_2$O)$_2$(B-α-GeW$_9$O$_{34}$)$_2$]$^{8-}$ were isolated [37,38]. As a part of our work, in this paper, we report three new sandwich-type POTs decorated by Ni^{II}-aromatic amine complexes [Ni(2,2′-bpy)$_2$(H$_2$O)][{Ni(2,2′-bpy)$_2$(H$_2$O)}$_2${Ni(2,2′-bpy)}$_2${Ni$_4$(H$_2$O)$_2$(B-α-PW$_9$O$_{34}$)$_2$}]·3H$_2$O (**1**), [Ni(2,2′-bpy)$_3$][{Ni(2,2′-bpy)$_2$(H$_2$O)}$_2${Ni(2,2′-bpy)}$_2${Ni$_4$(H$_2$O)$_2$(B-α-AsW$_9$O$_{34}$)$_2$}]·2.5H$_2$O (**2**),

* Corresponding author. Fax: +86 378 3886876.
** Also corresponding author.
E-mail addresses: jpwang@henu.edu.cn (J.-P. Wang), jyniu@henu.edu.cn (J.-Y. Niu).

0022-4596/$ - see front matter © 2009 Elsevier Inc. All rights reserved.
doi:10.1016/j.jssc.2009.11.001

and $[Ni(2,2'\text{-bpy})_3]_2[\{Ni(2,2'\text{-bpy})_2(H_2O)\}_2\{Ni(2,2'\text{-bpy})\}_2\{Ni_4(H_2O)_2(B\text{-}\alpha\text{-}Ge\text{-}W_9O_{34})_2\}]\cdot 6H_2O$ (**3**). To the best of our knowledge, **1**–**3** represent a rare family of sandwich-type POTs decorated by Ni^{II}-aromatic amine complexes in POM chemistry. The successful syntheses of these POMs not only further testify that the functionalization of sandwich-type POMs by aromatic amine ligands is an effective strategy in preparing novel inorganic–organic hybrid TMSPs, but also enrich the structural diversity of sandwich-type TMSPs. Furthermore, the preparations of **1**–**3** provide the likelihood to introduce other electron-delocalized aromatic ligands (such as polycarboxylic ligands) to the system of sandwich-type POMs. We believed that the expedited development of such hybrid sandwich-type POMs constructed from high-nuclear metal cluster aggregations or their multi-dimensional POM derivatives decorated by electron-delocalized aromatic ligands will be promoted greatly in due time.

2. Experimental

2.1. Materials and methods

$Na_{12}[P_2W_{15}O_{56}]\cdot 18H_2O$ precursors were prepared according to previous literature [39] and confirmed by IR spectra. Other chemical reagents were used as commercially purchased without further purification. Elemental analyses (C, H and N) were performed using a Perkin-Elmer 2400 Elemental Analyzer. Inductively coupled plasma (ICP) analysis was performed on a Perkin-Elmer Optima 2000 ICP-OES spectrometer. IR spectra were obtained on a sample powder palletized with KBr on Nicolet AVATAR 360 FTIR spectrophotometer over the range 4000–400 cm^{-1}. Variable temperature magnetic susceptibilities were carried out with a Quantum Design MPMS-5 magnetometer. Experimental susceptibilities were corrected for diamagnetism of the constituent atoms by use of Pascal's constants.

2.2. Synthesis

2.2.1. Synthesis of $[Ni(2,2'\text{-bpy})_2(H_2O)][\{Ni(2,2'\text{-bpy})_2(H_2O)\}_2\{Ni(2,2'\text{-bpy})\}_2\{Ni_4(H_2O)_2(B\text{-}\alpha\text{-}PW_9O_{34})_2\}]\cdot 3H_2O$ (1)

A mixture of $Na_{12}P_2W_{15}O_{56}\cdot 18H_2O$ (0.432 g, 0.10 mmol), $NiSO_4\cdot 6H_2O$ (0.158 mL, 0.60 mmol), $BaCl_2\cdot 2H_2O$ (0.125 g, 0.50 mmol), 2,2′-bipyridine (0.045 g, 0.29 mmol) and water (15 mL) was stirred and its pH value was adjusted to 5.3 with 2 M HCl. The resulting suspension was sealed in a 23 mL Teflon-lined reactor and kept at 160 °C for four days. After cooling the autoclave to room temperature over two days by a programmable temperature-controlling instrument, green block single crystals of **1** were separated, washed with water and air-dried (32% yield based on W element). Elemental analysis (%) calcd $C_{80}H_{80}N_{16}Ni_9P_2W_{18}O_{76}$: C, 15.06; N, 3.51; H, 1.26; Ni, 8.28; P, 0.97; W, 51.86. Found: C, 14.96; N, 3.46; H, 1.27; Ni, 8.18; P, 1.00; W, 52.24. IR (KBr pellet) (cm^{-1}): 497(m), 597 (m), 668(s), 736(s), 770(s), 789(s), 897(s), 942(s), 970(s), 1049(s), 1159(m), 1107(m), 1383(m), 1440(s), 1474(s), 1628(m), 3437(w).

2.2.2. Synthesis of $[Ni(2,2'\text{-bpy})_3][\{Ni(2,2'\text{-bpy})_2(H_2O)\}_2\{Ni(2,2'\text{-bpy})\}_2\{Ni_4(H_2O)_2(B\text{-}\alpha\text{-}AsW_9O_{34})_2\}]\cdot 2.5H_2O$ (2)

A mixture of $Na_3AsO_4\cdot 12H_2O$ (0.594 g, 1.40 mmol), $Na_2WO_4\cdot 2H_2O$ (4.288 g, 13.00 mmol), $NiCl_2\cdot 6H_2O$ (0.259 g, 1.09 mmol), $Ni(CH_3COO)_2\cdot 6H_2O$ (0.285 g, 1.00 mmol), 2,2′-bipyridine (0.30 g, 1.92 mmol) and water (15 mL) was stirred for an hour at 90 °C and its pH value was adjusted to 5.6 with 2 M HCl. The resulting suspension was sealed in a 23 mL Teflon-lined reactor and kept at 180 °C for six days. After cooling the autoclave to room temperature over two days by a programmable temperature-controlling instrument, green block single crystals of **2** were separated, washed with distilled water and air-dried in 28% yield based on W element. Elemental analysis (%) calcd for $C_{90}H_{85}N_{18}Ni_9As_2W_{18}O_{74.50}$: C, 16.38; N, 3.82; H, 1.30; Ni, 8.01; As, 2.27; W, 50.15. Found: C, 16.29; N, 3.78; H, 1.33; Ni, 7.94; Ge, 2.22; W, 50.68. IR (KBr pellet) (cm^{-1}): 762(s), 780(s), 853(s), 902(s), 960(s), 1167(m), 1277(m), 1314(m), 1448(s), 1629(s), 3420 (w).

2.2.3. Synthesis of $[Ni(2,2'\text{-bpy})_3]_2[\{Ni(2,2'\text{-bpy})_2(H_2O)\}_2\{Ni(2,2'\text{-bpy})\}_2\{Ni_4(H_2O)_2(B\text{-}\alpha\text{-}GeW_9O_{34})_2\}]\cdot 6H_2O$ (3)

A mixture of $Na_2WO_4\cdot 2H_2O$ (0.595 g, 1.80 mmol), GeO_2 (0.021 g, 0.20 mmol), $NiSO_4\cdot 6H_2O$ (0.105 g, 0.40 mmol), 2,2′-bipyridine (0.062 g, 0.40 mmol) and water (15 mL) was stirred and the pH adjusted to 5.9 with 2 M HCl. The resulting suspension was sealed in a 23 mL Teflon-lined reactor and kept at 160 °C for eight days. After cooling the autoclave to room temperature over two days by a programmable temperature-controlling instrument, green block crystals of **3** were separated, washed with water and air-dried (ca. 21% yield based on W element). Elemental analysis (%) calcd for $C_{120}H_{116}N_{24}Ni_{10}Ge_2W_{18}O_{78}$: C, 20.06; N, 4.68; H, 1.63; Ni, 8.17; Ge, 2.02; W, 46.07. Found: C, 20.09; N, 4.66; H, 1.67; Ni, 8.18; Ge, 1.97; W, 46.54. IR (KBr pellet) (cm^{-1}): 703(s), 779(s), 832(s), 865(m), 881(s), 935(s), 1154(m), 1393(m), 1443(s), 1635(s), 3429 (w).

2.3. X-ray structure determination

A crystal with dimensions $0.18\times 0.12\times 0.10\,mm^3$ for **1** $0.13\times 0.12\times 0.10\,mm^3$ for **2** and $0.20\times 0.15\times 0.12\,mm^3$ for **3**, was stuck on a glass fiber and intensity data were collected at 296 K on a Bruker Smart APEX II CCD diffractometer with graphite-monochromated Mo-$K\alpha$ radiation (λ=0.71073 Å). Routine Lorentz polarization and Multi-scan absorption correction were applied to intensity data. Their structures were determined and the heavy atoms were found by direct methods using the SHELXTL-97 program package [40,41]. The remaining atoms were found from successive full-matrix least-squares refinements on F^2 and Fourier syntheses. No hydrogen atoms associated with water molecules were located from the difference Fourier maps. Positions of the hydrogen atoms attached to carbon and nitrogen atoms were geometrically placed. All hydrogen atoms were refined isotropically as a riding mode using the default SHELXTL parameters. For **1**, of 19 773 reflections, 10 900 unique reflections (R_{int}=0.0754) were considered observed [$I > 2\sigma(I)$]. The final cycle of refinement including atomic coordinates and the anisotropic thermal parameters converged to R_1=0.0482 and wR_2=0.1164 [$I > 2\sigma(I)$]. For **2**, of 32 910 reflections, 11 624unique reflections (R_{int}=0.0344) were considered observed [$I > 2\sigma(I)$]. The final cycle of refinement including atomic coordinates and the anisotropic thermal parameters converged to R_1=0.0294 and wR_2=0.0689 [$I > 2\sigma(I)$]. For **3**, of 27 515 reflections, 13 135 unique reflections (R_{int}=0.2101) were considered observed [$I > 2\sigma(I)$]. The final cycle of refinement including atomic coordinates and the anisotropic thermal parameters converged to R_1=0.0653 and wR_2=0.1336 [$I > 2\sigma(I)$]. Crystallographic data and structure refinements for **1**–**3** are summarized in Table 1. Selected bond lengths for **1**–**3** are given in Table 2.

3. Results and discussion

3.1. Synthesis

1, **2** and **3** were all synthesized under hydrothermal conditions (Table 3). **1** was synthesized by reaction of trilacunary

Table 1
The crystallographic data and structure refinements of **1**–**3**.

	1	2	3
empirical	$C_{80}H_{80}N_{16}Ni_9$	$C_{90}H_{85}N_{18}Ni_9$	$C_{120}H_{116}N_{24}Ni_{10}$
formula	$P_2W_{18}O_{76}$	$As_2W_{18}O_{74.50}$	$Ge_2W_{18}O_{78}$
fw	6381.23	6598.29	7183.95
cryst system	monoclinic	monoclinic	triclinic
space group	*C*2/*c*	*C*2/*c*	$P\bar{1}$
a (Å)	29.462(6)	29.500(3)	15.6436(13)
b (Å)	24.713(5)	24.804(2)	17.0693(14)
c (Å)	18.087(4)	18.1476(16)	19.0695(16)
α (deg)			63.6470(10)
β (deg)	94.17(3)	94.3390(10)	72.6590(10)
γ (deg)			66.2240(10)
vol (Å^3)	13134(5)	13241(2)	4131.3(6)
Z	4	4	1
Temp (K)	296(2)	296(2)	296(2)
d_{calcd} (g cm^{-3})	3.227	3.310	2.888
abs coeff (mm^{-1})	17.070	17.408	14.032
index range	$-35 \le h \le 34$ $-29 \le k \le 29$ $0 \le l \le 21$	$-34 \le h \le 34$ $-25 \le k \le 29$ $-21 \le l \le 21$	$-18 \le h \le 18$ $-20 \le k \le 19$ $-22 \le l \le 22$
measured refIns	19 773	32 910	27 515
unique refIns	10 900	11 624	13 135
R_{int}	0.0754	0.0344	0.2101
wavelength (Å)	0.71073	0.71073	0.71073
crystal size (mm^3)	0.18 × 0.12 × 0.10	0.13 × 0.12 × 0.10	0.20 × 0.15 × 0.12
GOF on F^2	1.032	1.015	1.009
R_1[a] [$I > 2\sigma(I)$]	0.0482	0.0294	0.0653
wR_2[b] [$I > 2\sigma(I)$]	0.1105	0.0658	0.1244
R_1[a] (all data)	0.0618	0.0400	0.0838
wR_2[b] (all data)	0.1164	0.0689	0.1336

[a] $R_1 = \sum \| F_o| - |F_c \| / \sum |F_o|$.
[b] $wR_2 = [\sum w(F_o^2 - F_c^2)^2 / \sum w(F_o^2)^2]^{1/2}$;
$w = 1/[\sigma^2(F_o^2) + (xP)^2 + yp]$, $p = (F_o^2 + 2F_c^2)/3$, where x=0.0563, y=359.4996 for **1**, x=0.0281, y=103.5251 for **2** and x =0.0121, y=0 for **3**.

Dawson-type precursor $[P_2W_{15}O_{56}]^{12-}$ with the $NiSO_4 \cdot 6H_2O$ in the presence of 2,2′-bpy under hydrothermal conditions. Interestingly, the Keggin-type fragments are observed in **1**, indicating that the following transformation must have taken place in the formation of **1**: $[P_2W_{15}O_{56}]^{12-} \rightarrow [B\text{-}\alpha\text{-}PW_9O_{34}]^{9-}$. As a result, the polyoxoanion $[P_2W_{15}O_{56}]^{12-}$ is metastable in the course of the hydrothermal reaction and undergoes a disassembly and reassembly course at the certain pH value (5.3). In contrast, **2** and **3** were isolated without using any POM precursors, but directly by employing the initial oxides or salts including their component elements and aromatic amine ligands. If $NiSO_4 \cdot 6H_2O$ was replaced by $CuCl_2 \cdot 2H_2O$ in the synthesis of **3**, a novel hexa-Cu sandwiched tungstogermanate {[Cu(2,2′-bpy)]$_2$[Cu(2,2′-bpy)$_2$]$_2$[Cu$_6$(2,2′-bpy)$_2$ (B-α-GeW$_9$O$_{34}$)$_2$]} [37] was afforded, which is decorated by four $[Cu(2,2'\text{-bpy})_2]^{2+}$ coordination cations, and notice that the most striking structural feature is that two peripheral Cu atoms on the {Cu$_6$} cluster were also functionalized by two 2,2′-bpy ligands. When 2,2′-bpy ligand was replaced by phen, an isostructural tungstogermanate was obtained [37]. In our case, parallel experiments reveal that initial TM reactants have a great influence on the crystallization phases and the structural types of products. For example, in the preparation of **3**, when the initial reactant $NiSO_4 \cdot 6H_2O$ was replaced by $CoSO_4 \cdot 7H_2O$ and 1,6-hexamethylenediamine was introduced to the reaction system at 160 °C, another hexa-cobalt sandwiched tungstogermanate $(C_6N_2H_{18})_3H_2$ [{Co(2,2′-bpy)}$_2$Co$_4$(H$_2$O)$_2$(α-GeW$_9$O$_{34}$)$_2$]·4H$_2$O was isolated [38], in which the two peripheral Co atoms on the {Co$_6$} cluster are chelated by two 2,2′-bpy ligands and protonated 1,6-hexamethylenediamine components only act as countercations due to the case that it is very difficult for such long carbon chain amines to chelate nickel ions. It should be noted that these structural motifs are evidently different from those previously reported 2-D sandwich-type POTs, where 2-D extended (4,4)-topological networks are constructed by tetra-Ni^{II}-substituted sandwich-type POMs and Ni^{II}-aliphatic amine bridges [34]. The main reason may be that flexible aliphatic amine ligands prefer to coordinate to TM ions and the resulting TM-aliphatic amine ions are easy to act as bridges to construct

Table 2
Selected bond length (Å) for **1**–**3**.

1			
P(1)–O(31)	1.556(5)	P(1)–O(32)	1.552(6)
P(1)–O(33)	1.532(6)	P(1)–O(34)	1.549(6)
Ni(1)–O(12)	2.022(6)	Ni(1)–O(20)	2.056(6)
Ni(1)–N(1′)	2.036(7)	Ni(1)–O(15)	2.184(6)
Ni(1)–N(1)	2.040(7)	Ni(1)–O(14)	2.198(6)
Ni(2)–O(2)	2.035(7)	Ni(2)–N(3′)	2.067(9)
Ni(2)–N(3)	2.058(10)	Ni(2)–N(2)	2.086(9)
Ni(2)–N(2′)	2.063(10)	Ni(2)–O(1W)	2.124(7)
Ni(3)–O(28)	1.983(6)	Ni(3)–O(27)	2.064(6)
Ni(3)–O(25)#1	1.995(6)	Ni(3)–O(34)#1	2.149(6)
Ni(3)–O(26)#1	2.050(6)	Ni(3)–O(34)	2.150(5)
Ni(4)–O(29)#1	2.000(6)	Ni(4)–O(2W)	2.078(6)
Ni(4)–O(30)#1	2.007(6)	Ni(4)–O(27)	2.082(6)
Ni(4)–O(26)	2.060(5)	Ni(5)–O(3W)	2.084(11)
Ni(5)–O(3W)#2	2.084(11)	Ni(5)–N(4′)	2.133(11)
Ni(5)–N(4′)#2	2.133(11)	Ni(5)–N(4)#2	2.224(9)
Ni(5)–N(4)	2.224(9)	Ni(4)–O(34)#1 1	2.191(6)
2			
As(1)–O(31)	1.678(5)	As(1)–O(32)	1.692(6)
As(1)–O(33)	1.671(5)	As(1)–O(34)	1.680(5)
Ni(1)–O(25)#1	1.985(5)	Ni(1)–O(27)	2.106(5)
Ni(1)–O(28)	2.005(5)	Ni(1)–O(34)#1 1	2.123(5)
Ni(1)–O(26)#1	2.084(5)	Ni(1)–O(34)	2.127(5)
Ni(2)–O(29)#1	2.023(6)	Ni(2)–O(27)	2.082(5)
Ni(2)–O(30)#1	2.029(5)	Ni(2)–O(26)	2.083(5)
Ni(2)–O(1W)	2.055(6)	Ni(2)–O(34)#1 1	2.144(5)
Ni(3)–N(1′)	2.020(7)	Ni(3)–N(1)	2.065(7)
Ni(3)–O(10)	2.033(5)	Ni(3)–O(14)	2.158(6)
Ni(3)–O(20)	2.061(5)	Ni(3)–O(15)	2.193(5)
Ni(4)–O(7)	2.039(5)	Ni(4)–N(3)	2.087(10)
Ni(4)–N(2′)	2.049(8)	Ni(4)–N(2)	2.090(9)
Ni(4)–N(3′)	2.076(8)	Ni(5)–N(4)	1.99(4)
Ni(5)–N(4′)	2.0000(10)	Ni(5)–N(5)#2	2.05(4)
Ni(5)–N(5)	2.07(4)	Ni(5)–N(4)#2	2.16(4)
Ni(5)–N(4′)#2	2.26(2)	Ni(4)–O(2W)	2.134(7)
3			
Ge(1)–O(31)	1.761(9)	Ge(1)–O(32)	1.759(9)
Ge(1)–O(33)	1.797(9)	Ge(1)–O(34)	1.728(9)
Ni(1)–O(20)	2.028(9)	Ni(1)–N(1′)	2.080(13)
Ni(1)–N(1)	2.035(13)	Ni(1)–O(14)	2.175(9)
Ni(1)–O(12)	2.053(10)	Ni(1)–O(15)	2.194(10)
Ni(2)–O(2)	2.015(10)	Ni(2)–N(2′)	2.091(14)
Ni(2)–N(3)	2.049(13)	Ni(2)–N(3′)	2.100(16)
Ni(2)–N(2)	2.055(15)	Ni(2)–O(1W)	2.114(11)
Ni(3)–O(25)	2.013(9)	Ni(3)–O(34)#1 1	2.072(9)
Ni(3)–O(28)	2.042(9)	Ni(3)–O(26)	2.118(10)
Ni(3)–O(34)	2.058(8)	Ni(3)–O(27)#1 1	2.147(11)
Ni(4)–O(29)	2.046(8)	Ni(4)–O(27)	2.068(9)
Ni(4)–O(30)	2.054(9)	Ni(4)–O(2W)	2.088(12)
Ni(4)–O(34)#1	2.064(10)	Ni(4)–O(26)	2.096(9)
Ni(5)–N(4)	2.104(16)	Ni(5)–N(4′)	2.099(15)
Ni(5)–N(5)	2.065(13)	Ni(5)–N(5′)	2.094(17)
Ni(5)–N(6)	2.075(17)	Ni(5)–N(6′)	2.097(14)

Symmetry transformations used to generate equivalent atoms: (**1**); #1–*x*+1/2, –*y*+1/2, –*z*; #2–*x*+1, –*y*, –*z*+1 (**2**)#1–*x*+1/2, –*y*–1/2, –*z*; #2–*x*, –*y*, –*z*+1; (**3**)#1–*x*+3, –*y*+1, –*z*+1.

Table 3
Summary of synthetic conditions and related compounds in the preparations of **1**–**3**.

Initial reactants (molar ratio)	Temperature (°C)	Phases
$Na_{12}P_2W_{15}O_{56}\cdot 18H_2O/NiSO_4\cdot 6H_2O/BaCl_2/2,2'$-bpy/$H_2O$=0.1/0.6/0.5/0.29/833	160	**1**
$Na_2WO_4\cdot 2H_2O/GeO_2/CuCl_2\cdot 2H_2O/2,2'$-bpy/$H_2O$=1.9/1.15/0.3/0.32/833	180	{[Cu(2,2′-bpy)]$_2$[Cu(2,2′-bpy)$_2$]$_2$[Cu$_6$(2,2′-bpy)$_2$(B-α-$GeW_9O_{34})_2$]}[11a]
$Na_2WO_4\cdot 2H_2O/GeO_2/CoSO_4\cdot 7H_2O$/1,6-hexamethylenediamine/2,2′-bpy/H_2O=1.8/0.2/0.4/0.4/0.4/833	160	$(C_6N_2H_{18})_3H_2$[{Co(2,2′-bpy)}$_2$Co$_4$(H_2O)$_2$(α-$GeW_9O_{34})_2]\cdot 4H_2O$[11b]
K_8Na_2[A-α-$GeW_9O_{34}]\cdot 25H_2O/NiCl_2\cdot 6H_2O$/1,2-diaminopropane(dap)/H_2O=0.08/1.0/2.945/444	100	{[Ni(dap)$_2$(H_2O)]$_2$[Ni(dap)$_2$]$_2$[Ni$_4$(Hdap)$_2$(α-B-$HGeW_9O_{34})_2$]}$\cdot 6H_2O$[9a]
$Na_2WO_4\cdot 2H_2O/Na_3AsO_4\cdot 12H_2O/NiCl_2\cdot 6H_2O/Ni(CH_3COO)_2\cdot 6H_2O$/2,2′-bpy/$H_2O$=13/1.4/1.09/1.0/1.92/833	90	**2**
Na_2WO_4. $2H_2O/GeO_2/NiSO_4\cdot 6H_2O$/2,2′-bpy/$H_2O$=1.8/0.2/0.4/0.4/833	160	**3**
$Na_{12}P_2W_{15}O_{56}\cdot 18H_2O/NiCl_2\cdot 6H_2O$/1,2-diaminopropane(dap)/H_2O=0.05/0.395/1.178/278	120	{[Ni(dap)$_2$(H_2O)]$_2$[Ni(dap)$_2$]$_2$[Ni$_4$(Hdap)$_2$(α-B-$HPW_9O_{34})_2$]}$\cdot 4H_2O$[9a]

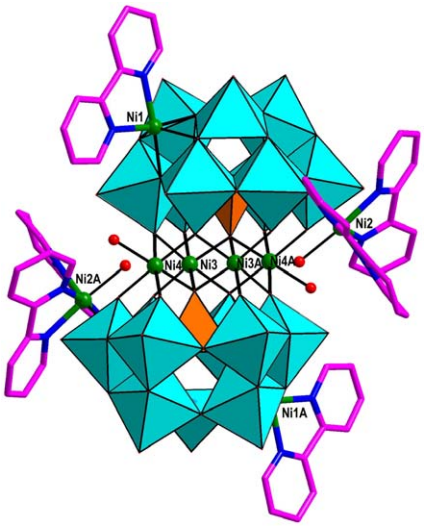

Fig. 1. Combined polyhedral/ball-and-stick/wire representation of polyoxoanion in **1**. The atoms with "A" in their labels are symmetrically generated (A: 0.5–*x*, 0.5–*y*, –*z*). Hydrogen atoms were omitted for clarity. Color codes: Orange, PO_4; Turquiose, WO_6. (For interpretation of the references to color in this figure legend, the reader is referred to the web version of this article.)

extended structures, whereas it is very difficult for TM-aromatic amine ions to serve as bridges forming extended architectures due to larger steric hindrance though rigid aromatic amines can also bond to TM ions. Therefore, the systematic exploration on the functionalization of TMSPs by aromatic N-containing ligands remains a great challenge to us. The continuous work is in progress.

3.2. Structural description

Single-crystal X-ray diffraction reveals that **1** and **2** crystallize in the monoclinic space group *C*2/*c*, whereas **3** crystallizes in the triclinic space group $P\bar{1}$. Although the crystal systems and space groups of **1–2** and **3** are different, their polyoxoanions {Ni(2,2′-bpy)$_2$(H_2O)}$_2${Ni(2,2′-bpy)}$_2$ {$Ni_4(H_2O)_2$(B-α-$XW_9O_{34})_2$}]$^{n-}$ (X=P^V, n=4 for **1**; X=As^V, n=4 for **2**; X=Ge^{IV}, n=4 for **3**) display the same structural framework and are all composed of a well-known sandwich-type entity [$Ni_4(H_2O)_2$(B-α-$XW_9O_{34})_2$]$^{n-}$ as well as decorated two [Ni(2,2′-bipy)]$^{2+}$ and two [Ni(2,2′-bpy)(H_2O)]$^{2+}$ coordination cations (Fig. 1, S1, S2). Therefore, only the structure of **1** is described in detail.

The structural unit of **1** consists of a tetra-supporting polyoxoanion fragment [{Ni(2,2′- bpy)$_2$(H_2O)}$_2${Ni(2,2′-bpy)}$_2$ {$Ni_4(H_2O)_2$(B-α-$GeW_9O_{34})_2$}]$^{4-}$, two discrete [Ni(2,2′-bpy)$_3$]$^{2+}$ cations and six lattice water molecules. Notice that the most striking structural feature of the polyoxoanion [{Ni(2,2′-bpy)$_2$(H_2O)}$_2${Ni(2,2′-bpy)}$_2${$Ni_4(H_2O)_2$(B-α- $GeW_9O_{34})_2$}]$^{4-}$ in **1** is that a classical Weakley sandwich-type moiety [$Ni_4(H_2O)_2$(B-α-$GeW_9O_{34})_2$]$^{12-}$ is decorated by four nickel-aromatic amine complexes, namely two [Ni(2,2′-bpy)$_2$(H_2O)]$^{2+}$ and two [Ni(2,2′-bpy)]$^{2+}$ complex cations. In the skeleton of sandwich-type polyoxoanion, each of the two [Ni(2,2′-bpy)(H_2O)]$^{2+}$ fragments coordinates to the 'belt' position of the B-α-[GeW_9O_{34}]$^{10-}$ subunits through a terminal oxygen atom, while each of the two [Ni(2,2′-bpy)]$^{2+}$ fragments grafts on the 'polar' position of the two B-α-[GeW_9O_{34}]$^{10-}$ subunits via four bridging oxygen atoms. Notably, the grafting fashion of the [Ni(2,2′-bpy)]$^{2+}$ cation is very rarely observed in the system of POM and TM-aliphatic amine cations. But similar grafting fashion of the [Cu(2,2′-bpy)]$^{2+}$ cation has been observed in our previously reported hybrid inorganic–organic POT Na[{Cu(2,2′-bpy)(H_2O)}$_2${Cu(2,2′-bpy)}$_2$(B-α-SbW_9O_{33})]$\cdot 2H_2O$ [42], where each [Cu(2,2′-bpy)]$^{2+}$ group grafts on a window on the 'polar' position of [B-α-SbW_9O_{33}]$^{9-}$ unit by four μ_3-O bridges.

Recently, organic–inorganic hybrid sandwich-type POTs have attracted increasing interest and developed as a unique subclass of TMSPs. For example, in 2006, we reported the first hybrid 1-D chain-like sandwich-type germanotungstate [Cu(en)$_2$]$_3$[Cu(en)$_2$(H_2O)]$_2${[$Cu_4(GeW_9O_{34})_2$] [Cu(en)$_2$]}$\cdot 9.5H_2O$ (Fig. 2a) [33]. In 2007, Yang et al. reported a series of 2-D hybrid networks constructed from tetra-TM sandwiched POTs and TMCs bridges (Fig. 2b) [34,35]. In 2008, Yang et al. prepared a family of novel hybrid high-nuclear-TM sandwiched TMSPs with 0-D, 2-D and 3-D structures, in which the number of TM cations in the sandwich belts varies from tetra-nuclear to octa-nuclear [43–46]. In the same year, Wang et al. addressed two extended structural phosphotungstates $(NH_4)_2$[Ni_4(enMe)$_8$(H_2O)$_2$$Ni_4$(enMe)$_2$($PW_9O_{34})_2$]$\cdot 9H_2O$ and $Na_2[H_6N_2(CH_2)_6]_2$ {$Ni_4[H_4N_2(CH_2)_6]_2(H_2PW_9O_{34})_2$}$\cdot 7H_2O$ (Fig. 2c) constructed from tetra-Ni-substituted sandwich-type POMs [36]. Subsequently, we reported a 1-D sinusoidal chain-like tungsto-antimonate $Na_4H_7[Na_3(H_2O)_6Mn_3(\mu$-OAc)$_2$($B$-α-$SbW_9O_{33})_2]\cdot 20H_2O$ (Fig. 2d) consisting of sandwich-type POTs bridged by the carboxylate-bridging ligands [47], and Dolbecq et al. synthesized two novel hybrid tungstoantimonates $Na_{14}[Fe^{III}_4(ox)_4(H_2O)_2(SbW_9O_{33})_2]\cdot 60H_2O$ (Fig. 2e) and $[enH_2]_7[Fe^{III}_4(ox)_4(SbW_9O_{33})_2]\cdot 14H_2O$, in which tetra-nuclear Fe^{III} clusters in the sandwich belt are functionalized by oxalato ligands [48]. As shown above, most hybrid sandwich-type TMSPs are decorated by TM-aliphatic amine complexes or TM-carboxylate complexes. However, the exploration on hybrid sandwich-type POTs decorated by TM-aromatic amine complexes is less developed (Fig. 2f) [37,38]. As far as we know, **1**, **2** and **3**

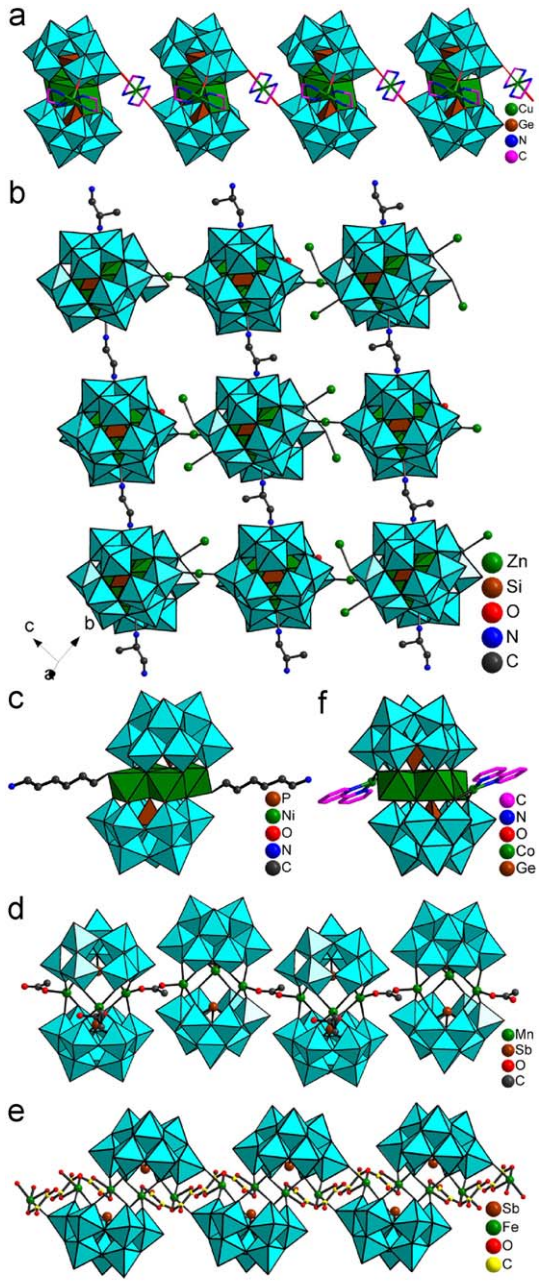

Fig. 2. Main structural types of organic–inorganic hybrid sandwich-type POTs. Color codes: Turquiose octahedra, WO_6; Orange tetrahedral, XO_4; Green octahedra, first row transition-metal cations MO_6. (For interpretation of the references to color in this figure legend, the reader is referred to the web version of this article.)

represent rare examples of the organic–inorganic hybrid sandwich-type TMSPs functionalized by multiple nickel-aromatic amine complexes.

In the structural unit of **1**, there are five crystallographically unique Ni^{2+} cations. Both Ni1 and Ni2 complex cations all graft on the polyoxoanion skeleton via four bridging oxygen atoms and a terminal oxygen atom, respectively; Ni3 and Ni4 ions fused together with their symmetrical atoms form a rhombic $\{Ni_4\}$ cluster by edge-sharing fashion; whereas the Ni5 complex cation act as a discrete countercation. Albeit the five crystallographically unique Ni^{II} atoms all reside in the distorted octahedral geometries, they display four kinds of octahedrally environments in **1**: the Ni1 ion is bonded to four oxygen donors

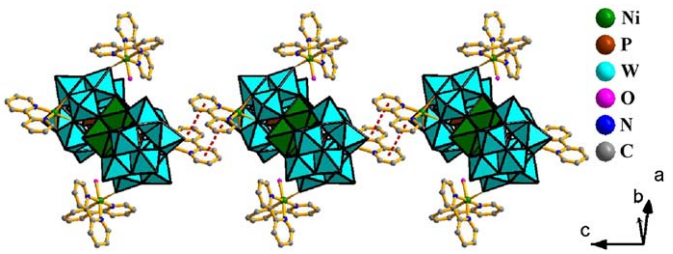

Fig. 3. The π–π stacking fashion of polyoxoanions in **1** along the *c* axis. Hydrogen atoms were omitted for clarity. Color codes: Orange, PO_4; Turquiose, WO_6; Green, NiO_6. (For interpretation of the references to color in this figure legend, the reader is referred to the web version of this article.)

from $[B\text{-}\alpha\text{-}GeW_9O_{34}]^{10-}$ fragment and two nitrogen atoms from one 2,2′-bpy [Ni–O: 2.022 (6)–2.198(6) Å and Ni–N: 2.036(7)–2.040(7) Å]; the octahedral geometry of the Ni2 ion is defined by one terminal water ligand, one oxygen atom from the $[B\text{-}\alpha\text{-}GeW_9O_{34}]^{10-}$ skeleton and four nitrogen donors from two 2,2′-bpy ligands [Ni–O: 2.035(7)–2.124(7) Å and Ni–N: 2.063(10)–2.860(9) Å]; both Ni3 and Ni4 ions are all coordinated by six oxygen atoms from bridging oxygen atoms or water molecule [Ni–O: 1.983(6)–2.191(6) Å]; and the Ni5 ion is combined with four nitrogen donors from two 2,2′-bpy ligands [Ni–N: 2.133(11)–2.224(9) Å] and two water molecules [Ni(5)–O(3W): 2.084 (11) Å]. Moreover, the separations of adjacent nickel atoms in the sides of the rhomb-like $\{Ni_4O_{16}\}$ cluster are between 3.151(2) and 3.163(2) Å, and the distances of two nickel atoms in the diagonals are between 3.158(2) and 5.466(2) Å. In comparison to **1**, the distances of nickel atoms in the rhomb-like Ni_4O_{16} groups of **2** and **3** become much longer and the lengths of the sides and diagonals of Ni_4O_{16} rhombs are in the range of 3.184(2)–3.192(2) Å and 3.243(3)–5.490(3) Å for **2** and 3.082(2)–3.117(3) Å and 3.106(3)–5.363(2) Å for **3**, respectively. The results indicate that the distances of Ni–Ni in the Ni_4O_{16} groups rise with increasing the electric charge of heteroatom, and the distances increase with increasing the radius of heteroatom when the charges of the heteroatoms are equal. Bond valence sum (BVS) [49] calculations for all the Ni and W atoms in **1**–**3**, the bond valence of these Ni and W atoms are +2 and +6, respectively.

It should be noted that every nickel ion bears one or two 2,2′-bpy ligands in the polyoxoanion skeletons of **1**−**3**, thus, stronger π–π interactions are likely to occur between 2,2′-bpy ligands. In the solid-state structure of **1**, adjacent polyoxoanions are closely aligned via the offsetting π–π interactions between neighboring 2,2′-bpy ligands on Ni1 and Ni2 along the *a* axis due to the centroid separations of adjacent 2,2′-bpy ligands being 3.7180(3) Å (Fig. 3), whereas the similar π–π interactions between neighboring 2,2′-bpy ligands were observed down the *c* axis with the centroid separations of adjacent 2,2′-bpy ligands being 3.6993 (9) Å for **2** and in the range of 3.696(3)–3.921(3) Å for **3** (Fig. S3 and S4). These observations are in approximate agreement with the previous study [50]. In addition, the 2,2′-bpy ligands on polyoxoanion skeleton and Ni5 are closely packed in the solid-state via the offsetting π–π interactions and multiple weak C–H…O hydrogen bonds forming 3-D supramolecular structure (Fig. 4), which contributes to the stability of the crystal structure.

3.3. IR spectra

The IR spectra of **1**–**3** have been recorded between 4000 and 400 cm^{-1}, which is very useful for the identification of characteristic vibration bands of trivacant Keggin polyoxoanions and organic components in products. For **1**–**3**, characteristic vibration patterns derived from α-Keggin-type polyoxoanions are observed

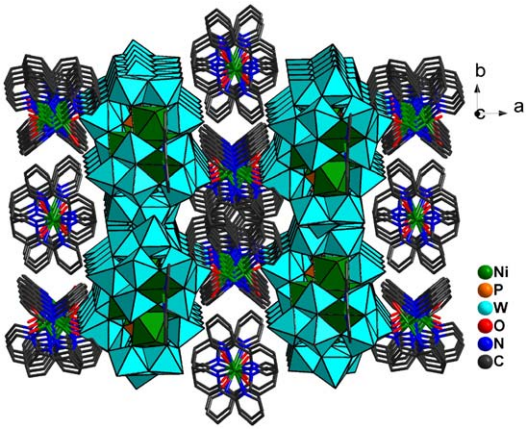

Fig. 4. The π–π stacking perspective viewed along *c* axis of crystal packing of **1**. Hydrogen atoms and water molecules were omitted for clarity. Color codes: Orange, PO_4; Turquiose, WO_6; Green, NiO_6. (For interpretation of the references to color in this figure legend, the reader is referred to the web version of this article.)

in 1100–700 cm^{-1} are in good agreement with the trivacant Keggin-type polyoxoanions [51,52]. The obvious characteristic bands, appearing at 942, 897, and 789 cm^{-1} for **1**, 960, 902, and 780 cm^{-1} for **2**, and 935, 881 and 779 cm^{-1} for **3**, are attributed to ν(W–Ot), ν(W–Ob), and ν(W–Oc), respectively. The vibration resonances observed in the region 1050–830 cm^{-1} for **1**–**3**, that is, 1049 cm^{-1} for **1**, 853 cm^{-1} for **2**, and 832 cm^{-1} for **3**, are assigned to ν(*X*–Oa) (*X*=P/As/Ge). Noted that these ν(*X*–Oa) vibration bands correlate very well to the *X*–Oa bond distances; namely, the ν(*X*–Oa) vibration frequency weakens with increasing the *X*–Oa distances (Table 2). In addition, the vibration bands at 1107, 1159, 1383, 1440, 1474 and 1628 cm^{-1} in **1** are indicative of the presence of 2,2′-bpy ligands. Similarly, the resonances at 1167, 1277, 1314, 1448 and 1629 cm^{-1} in **2** and 1154, 1393, 1443 and 1635 cm^{-1} in **3** are assigned to the characteristic vibration pattern of 2,2′-bpy ligands. According to previous investigations [51,52], the bands in the range of 1640–1560 cm^{-1} are assigned to anamorphic vibration and the vibration resonances in the range of 1600–1430 cm^{-1} are assigned to the ring framework vibration of 2,2′-bpy aromatic ligands; and the weak resonances between 1350 and 1000 cm^{-1} are attributed to C–N stretching modes. In addition, the broad peaks at 3440–3420 cm^{-1} are characteristic of water molecules in **1**–**3**.

3.4. Magnetic properties

Because the molecular structures of **1**, **2** and **3** are very similar, now, only the magnetic susceptibility of **1** is measured. The temperature dependence of the magnetic susceptibility of 1 under an applied field of 1 kOe is shown in Fig. 5 in the form of χ_m, $\chi_m T$ vs *T* plots. The χ_m value slowly increases from 0.0353 emu mol^{-1} at 300 K to 0.55 emu mol^{-1} at 26 K, then exponentially reaches the maximum value of 3.85 emu mol^{-1} at 2 K. The measured $\chi_M T$ value was 10.63 emu mol^{-1} K at room temperature, which is slightly larger than the only spin value (9.90 emu mol^{-1} K) for nine non-interacting Ni(II) ions (S=1, g=2.20). Upon cooling, the $\chi_M T$ value rises slowly until 50 K, subsequently rapidly increases, and finally reaches the maximum value 14.61 emu mol^{-1} K at 18 K. This behavior implies that ferromagnetic interactions occur within the rhomb-like Ni_4O_{16} cluster. Below 18 K, the $\chi_m T$ value sharply drops to 7.70 emu mol^{-1} K at 2 K, which results from the presence of the zero-field splitting within the ground state and intermolecular interactions. Additionally, the behavior of $\chi_M T$ at very low temperature may be related to an anisotropic coupling of the Ni^{II} ions inside the Ni_4O_{16} cluster rather than to a mean field correction [53]. Furthermore, the magnetic susceptibility data between 50 and 300 K follow the Curie–Weiss equation $\chi_m = C/(T-\theta)$ with C=10.286 emu mol^{-1} K and θ=14.176 K (Fig. 6). Such behavior manifests the predominant ferromagnetic interactions between adjacent Ni^{II} centers mediated by the oxygen bridges.

Considering the cluster topology and connection motif of magnetic centers in **1**, the ferromagnetic exchange interactions mainly occur in the rhomb-like tetranuclear Ni_4O_{16} core in the sandwich belt. Such ferromagnetic exchange interactions are frequently observed in high-nuclear nickel-oxo cluster compounds [28,53–56], which are largely due to the interactions between $^3A_2$ Ni^{II} ions. For example, the trinuclear-Ni^{II} clusters in $[Ni_3(H_2O)_3(PW_{10}O_{39})H_2O]^{7-}$ [28] and $[Ni_3Na(H_2O)_2(AsW_9O_{34})_2]^{11-}$ [53] exhibit the ferromagnetic exchange interactions. Furthermore, both the rhomb-like tetra-Ni^{II} cluster in $K_6Na_4[Ni_4(H_2O)_2(\alpha\text{-B-}PW_9O_{34})_2]\cdot 24H_2O$ [28] and the cubane Ni_4O_4 cluster in $Cs_2[H_2PW_9Ni_4O_{34}(OH)_3(H_2O)_6]\cdot 5H_2O$ [54] manifest the ferromagnetic couplings. Recently, several hexa-Ni^{II} cluster substituted POMs reported by Yang et al. also typify the ferromagnetic coupling interactions by means of the theoretical simulation [43]. Moreover, the magnetic property of the much larger nona-Ni^{II} cluster constructed by three Ni_3O_{12} triangles through two HPO_4^{2-} groups in $K_5Na_{11}[Ni_9(OH)_3(H_2O)_6(HPO_4)_2(PW_9O_{34})_3]\cdot 52H_2O$ was also investigated, which shows the dominant ferromagnetic interactions although it is a coexistence system of antiferromagnetic and ferromagne-

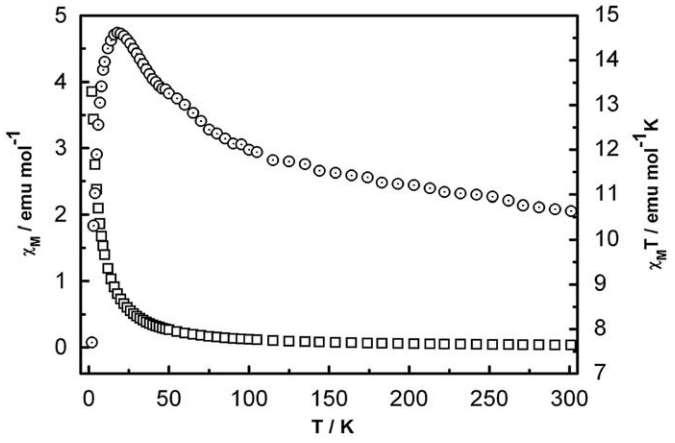

Fig. 5. The plots of χ_m and $\chi_m T$ vs *T* in the temperature of 2–300 K for **1**.

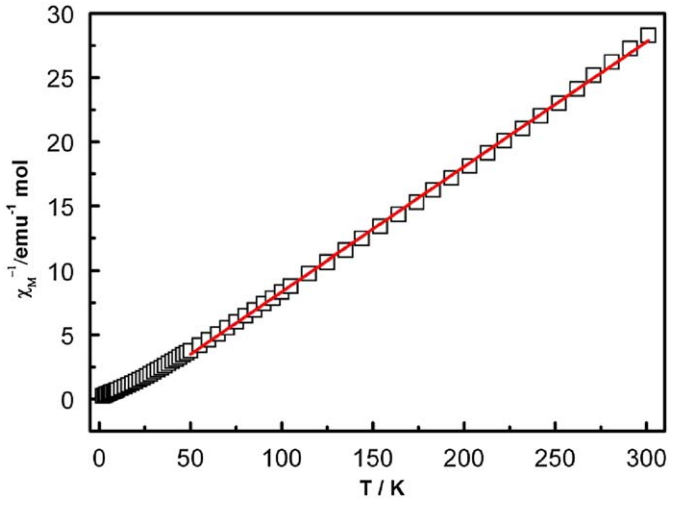

Fig. 6. The plot of χ_m^{-1} vs *T* in the temperature of 50–300 K for **1**. The red solid line represents the fit to experimental data.

tic interactions [55,56]. In fact, the magnetic interactions of nickel-oxo clusters are highly sensitive to the values of the Ni–O–Ni angles. In view of rhomb-like tetra-nuclear Ni_4O_{16} core in **1**, the ferromagnetic exchange interactions are expected in this system because the $Ni-O-Ni$ angles range from 93.1(2) to 100.1(1)°, which are in the range where the Ni–Ni ferromagnetic exchange interactions are dominant ($90\pm14^{\circ}$) by making use of magnetic coupling between the d_{x2-y2} orbitals on Ni^{2+} cations via the *p* orbitals on the bridging oxygen atoms [54].

4. Conclusions

Three new sandwich-type Polyoxotungstates functionalized by nickel-2,2′-bpy complexes $[Ni(2,2'\text{-bpy})_2(H_2O)][\{Ni(2,2'\text{-bpy})_2(H_2O)\}_2\{Ni(2,2'\text{-bpy})\}_2\{Ni_4(H_2O)_2(B\text{-}\alpha\text{-}PW_9O_{34})_2\}]\cdot 3H_2O$ (**1**), $[Ni(2,2'\text{-bpy})_3][\{Ni(2,2'\text{-bpy})_2(H_2O)\}_2\{Ni(2,2'\text{-bpy})\}_2\{Ni_4(H_2O)_2(B\text{-}\alpha\text{-}AsW_9O_{34})_2\}]\cdot 2.5H_2O$ (**2**), and $[Ni(2,2'\text{-bpy})_3]_2[\{Ni(2,2'\text{-bpy})_2(H_2O)\}_2\{Ni(2,2'\text{-bpy})\}_2\{Ni_4(H_2O)_2(B\text{-}\alpha\text{-}GeW_9O_{34})_2\}]\cdot 6H_2O$ (**3**) were successfully achieved, and which were structurally characterized by IR spectra, elemental analysis, and single-crystal X-ray diffraction. Notably, **1**–**3** represent the rare sandwich-type POTs functionalized by TM-aromatic amine coordination cations. Furthermore, the successful preparations of **1**–**3** provide the likelihood to introduce other electron-delocalized aromatic ligands (such as polycarboxylic ligands) to the system of sandwich-type POMs, which will pave an avenue for the design and syntheses of novel hybrid sandwich-type POMs constructed from high-nuclear metal cluster aggregations or their multi-dimensional POM derivatives decorated by electron-delocalized aromatic ligands under hydrothermal systems, and which will promote the expedited development of such hybrid sandwich-type POMs. Believe that large numbers of sandwich-type POMs decorated by electron-delocalized aromatic ligands will be obtained in due time.

Supplementary data

Crystallographic data for the structural analysis have been deposited with the Cambridge Crystallographic Data Center, CCDC numbers 661210–661212 for **1**–**3**. These data can obtained free of charge via http://www.ccdc.cam.ac.uk/data_request/cif or from The Cambridge Crystallographic Data Center, 12 Union Road, Cambridge CB2 1EZ, UK (Fax: +44-1223-336033; e-mail: deposit@ccdc.cam.ac.uk).

Acknowledgments

This work was supported by the Natural Science Foundation of China, the Foundation of Education Department of Henan Province, Natural Science Foundation of Henan Province and Natural Science Foundation of Henan University for financial support.

Appendix A. Supplementary material

Supplementary data associated with this article can be found in the online version at doi:10.1016/j.jssc.2009.11.001.

References

[1] M.T. Pope, A. Müller, Angew. Chem. Int. 30 (1991) 34–38.
[2] D.-L. Long, E. Burkholder, L. Cronin, Chem. Soc. Rev. 36 (2007) 105–121.
[3] M.T. Pope, A. Müller (Eds.), Polyoxometalates: From Platonic Solids to Anti-Retroviral Activity, Kluwer, Dordrecht, The Netherlands, 1994.
[4] T. Yamase, M.T. Pope, A. Müller (Eds.), Polyoxometalate Chemistry for Nano-Composite Design, Kluwer, Dordrecht, The Netherlands, 2002.
[5] M.T. Pope, A. Müller (Eds.), Polyoxometalate Chemistry: From Topology via Self-Assembly to Applications, Kluwer, Dordrecht, 2001.
[6] M.T. Pope, A. Müller (Eds.), Polyoxometalate: From Platonic Solids to Anti-Retroviral Activity, Kluwer, Dordrecht, 1994.
[7] A. Müller, F. Peters, M.T. Pope, D. Gatteschi, Chem. Rev. 98 (1998) 239–271.
[8] N. Mizuno, M. Misono, Chem. Rev. 98 (1998) 199–217.
[9] M. Sadakane, E. Steckhan, Chem. Rev. 98 (1998) 219–237.
[10] E. Coronado, C.J. Gomez-Garcia, Chem. Rev. 98 (1998) 273–296.
[11] J.T. Rhule, C.L. Hill, D.A. Judd, Chem. Rev. 98 (1998) 327–357.
[12] A. Müller, S. Roy, Coord. Chem. Rev. 245 (2003) 153–166.
[13] A. Müller, C. Serain, Acc. Chem. Res. 33 (2000) 2–10.
[14] X.F. Fang, T.M. Anderson, C. Benell, C.L. Hill, Chem. Eur. J. 11 (2005) 712–718.
[15] N.M. Okun, T.M. Anderson, C.L. Hill, J. Am. Chem. Soc. 125 (2003) 3194–3195.
[16] C.D. Wu, C.Z. Lu, H.H. Zhuang, J.S. Huang, J. Am. Chem. Soc. 124 (2002) 3836–3837.
[17] Y.H. Guo, C.W. Hu, X.L. Wang, Y.H. Wang, E.B. Wang, Y.N. Zhou, S.H. Feng, Chem. Mater. 13 (2001) 4058–4064.
[18] A.V. Besserguenev, M.H. Dickman, M.T. Pope, Inorg. Chem. 40 (2001) 2582–2586.
[19] X.-B. Cui, J.-Q. Xu, H. Meng, S.-T. Zheng, G.-Y. Yang, Inorg. Chem. 43 (2004) 8005–8009.
[20] H. Hussain, U. Kortz, Chem. Commun. (2005) 1191–1193.
[21] P. Mialane, A. Dolbecq, F. Sécheresse, Chem. Commun. (2006) 2485–3477.
[22] S.-T. Zheng, D.-Q. Yuan, H.-P. Jia, J. Zhang, G.-Y. Yang, Chem. Commun. (2007) 1858–1860.
[23] T.J.R. Weakly, H.T. Evans, J.S. Showell, G.F. Tourné, C.M. Tourné, J. Chem. Soc. Chem. Commun. 4 (1973) 139–140.
[24] R.G. Finke, M. Droege, J.R. Hutchinson, O. Gansow, J. Am. Chem. Soc. 103 (1981) 1587–1589.
[25] S.H. Wasfi, A.L. Rheingold, G.F. Kokoszka, A.S. Goldstein, Inorg. Chem. 26 (1987) 2934–2939.
[26] T.J.R. Weakley, R.G. Finke, Inorg. Chem. 29 (1990) 1235–1241.
[27] X. Zhang, Q. Chen, D.C. Duncan, R.J. Lachicotte, C.L. Hill, Inorg. Chem. 36 (1997) 4381–4386.
[28] L.H. Bi, E.B. Wang, J. Peng, R.D. Huang, L. Xu, C.W. Hu, Inorg. Chem. 39 (2000) 671–679.
[29] U. Kortz, S. Isber, M.H. Dickman, D. Ravot, Inorg. Chem. 39 (2000) 2915–2922.
[30] L.H. Bi, R.D. Huang, J. Peng, E.B. Wang, Y.H. Wang, C.W. Hu, J. Chem. Soc. Dalton Trans. (2001) 121–129.
[31] U. Kortz, S. Nellutla, A.C. Stowe, N.S. Dalal, U. Rauwald, W. Danquah, D. Ravot, Inorg. Chem. 43 (2004) 2308–2317.
[32] D. Drewes, E.M. Limanski, B. Krebs, Eur. J. Inorg. Chem. 44 (2005) 1542–1546.
[33] J.P. Wang, X.D. Du, J.Y. Niu, Chem. Lett. 35 (2006) 1408–1409.
[34] J.-W. Zhao, B. Li, S.-T. Zheng, G.-Y. Yang, Cryst. Growth Des. 7 (2007) 2658–2664.
[35] S.-T. Zheng, M.-H. Wang, G.-Y. Yang, Chem. Asian J. Chem. Asian J. 2 (2007) 1380–1387.
[36] Z. Zhang, J. Liu, E. Wang, C. Qin, Y. Li, Y. Qi, X. Wang, Dalton Trans. (2008) 463–468.
[37] J.P. Wang, J. Du, J.Y. Niu, CrystEngComm 10 (2008) 972–974.
[38] J.P. Wang, P.T. Ma, Y. Shen, J.Y. Niu, Cryst. Growth Des. 8 (2008) 3130–3133.
[39] R.G. Finke, M.W. Droege, P.J. Domaille, Inorg. Chem. 26 (1987) 3886–3896.
[40] G.M. Sheldrick, SHELXS97 Program for Crystal Structure Solution, University of Göttingen, Göttingen, Germany, 1997.
[41] G.M. Sheldrick, SHELXL97 Program for Crystal Structure Refinement, University of Göttingen, Göttingen, Germany, 1997.
[42] J.-P. Wang, P.-T. Ma, J. Li, J.-Y. Niu, Chem. Lett. 35 (2006) 994–995.
[43] J.-W. Zhao, H.–P. Jia, J. Zhang, S.-T. Zheng, G.-Y. Yang, Chem. Eur. J. 13 (2007) 10030–10045.
[44] S.-T. Zheng, D.-Q. Yuan, J. Zhang, G.-Y. Yang, Inorg. Chem. 46 (2007) 4569–4574.
[45] J.-W. Zhao, J. Zhang, S.-T. Zheng, G.-Y. Yang, Chem. Commun. (2008) 570–572.
[46] J.-W. Zhao, S.-T. Zheng, Z.-H. Li, G.-Y. Yang, Dalton Trans. (2009) 1300–1306.
[47] J.-P. Wang, P.-T. Ma, J. Li, H.-Y. Niu, J.-Y. Niu, Chem. Asian J. 3 (2008) 822–833.
[48] A. Dolbecq, J.-D. Compain, P. Mialane, J. Marrot, E. Rivière, F. Sécheresse, Inorg. Chem. 47 (2008) 3371–3378.
[49] I.D. Brown, D. Altermatt, Acta Crystallogr. Sect. B 41 (1985) 244–247.
[50] L. Lisnard, A. Dolbecq, P. Mialane, J. Marrot, E. Codjovi, F. Sécheresse, Dalton Trans. (2005) 3913–3920.
[51] A. Müller, S.Q.N. Shah, H. Bögge, M. Schmidtmann, Nature 397 (1999) 48–50.
[52] J.-W. Zhao, J. Zhang, S.-T. Zheng, G.-Y. Yang, J. Struct. Chem. 27 (2008) 933–942.
[53] I.M. Mbomekalle, B. Keita, M. Nierlich, U. Kortz, P. Berthet, L. Nadjo, Inorg. Chem. 42 (2003) 5143–5152.
[54] U. Kortz, A. Tézé, G. Hervé, Inorg. Chem. 38 (1999) 2038–2042.
[55] J.M. Clemente-Juan, E. Coronado, R. Galán-Mascarós, C.J. Gómez-García, Inorg. Chem. 38 (1999) 55–63.
[56] J.J. Borrás-Almenar, J.M. Clemente-Juan, E. Coronado, B.S. Tsukerblat, Inorg. Chem. 38 (1999) 6081–6088.